Real-Time Model Predictive Control for Shipboard Power Management Using the IPA-SQP Approach

Hyeongjun Park, Jing Sun, *Fellow, IEEE*, Steven Pekarek, *Fellow, IEEE*, Philip Stone, *Member, IEEE*, Daniel Opila, *Member, IEEE*, Richard Meyer, Ilya Kolmanovsky, *Fellow, IEEE*, and Raymond DeCarlo, *Fellow, IEEE*

***Abstract*— Shipboard integrated power systems, the key enablers of ship electrification, call for effective power management control (PMC) to achieve optimal and reliable operation in dynamic environments under hardware limitations and operational constraints. The design of PMC can be treated naturally in a model predictive control (MPC) framework, where a cost function is minimized over a prediction horizon subject to constraints. The real-time implementation of MPC-based PMC, however, is challenging due to computational complexity of the numerical optimization. In this paper, an MPC-based PMC for a shipboard power system is developed and its real-time implementation is investigated. To meet the requirements for real-time computation, an integrated perturbation analysis and sequential quadratic programming (IPA-SQP) algorithm is applied to solve a constrained MPC optimization problem. Several operational scenarios are considered to evaluate the performance of the proposed PMC solution. Simulations and experiments show that real-time optimization, constraint enforcement, and fast load following can be achieved with the IPA-SQP algorithm. Different performance attributes and their tradeoffs can be coordinated through proper tuning of the design parameters.**

***Index Terms*— Integrated perturbation analysis and sequential quadratic programming (IPA-SQP), integrated power system (IPS), model predictive control (MPC), power management control (PMC), real-time optimization.**

I. Introduction

SHIPBOARD integrated power systems (IPSs) have been pursued as the key enabling technology in ship electrification for applications including warships and high-value commercial ships [1], [2]. They provide electrical power for both the propulsion system and service loads, and rely on power management control (PMC) strategies to coordinate the power sources and loads to achieve efficient and robust operation and to meet various dynamic requirements in diverse and sometimes adverse conditions. Moreover, effective PMC strategies are expected to provide improved fuel efficiency, enhanced response speed, and superior reliability [3]. To accomplish this, PMC must effectively deal with nonlinear system dynamics and stringent constraints that protect system components. In addition, PMC must be simple to tune to be able to trade off and rebalance performance attributes. Several approaches have been proposed for shipboard PMC with IPS. An automatic rule-based expert system is proposed for reconfiguration of shipboard IPS to enhance survivability of naval ships in [4]. In [5], an automated self-healing strategy is investigated by solving an optimization problem with constraints using a linear programming algorithm. In [6], a decentralized control approach using an intelligent multiagent system for shipboard power systems is proposed.

Several research groups have developed shipboard PMC strategies using the real-time optimization framework. For example, a fast reconfiguration algorithm based on zone selection differential protection schemes is reported in [7]; however, [7] provides no evidence that the algorithm can be implemented in real time. In other studies, real-time simulations are achieved. For example, in [8], using the small population-based particle swarm optimization method, a fast intelligent reconfiguration algorithm is implemented on a real-time simulator. Seenumani *et al.* [9] pursue a methodology that exploits time-scale separation to achieve real-time optimization of a shipboard IPS. By solving a two-level simplified optimization problem, the computational efficiency is improved and these improvements are validated on a real-time simulator. In fact, studies of optimization-based PMC strategies typically demonstrate implementation feasibility using only real-time simulations. To the best of our knowledge, however, no study has demonstrated the feasibility of optimization-based PMC with test results on a physical platform.

In this paper, we design a PMC for a shipboard power system that includes multiple power sources and loads such as the ship propulsion system (SPS) and high-power electrical load (a pulsed-type load that represents an electromagnetic rail guns and/or an electromagnetic launch system). We consider

Manuscript received August 7, 2014; revised November 25, 2014; accepted January 10, 2015. Manuscript received in final form February 5, 2015. This work was supported by the Office of Naval Research under Contract N00014-09-D-0726. Recommended by Associate Editor E. Kerrigan. *(Corresponding author: Jing Sun.)*

H. Park and I. Kolmanovsky are with the Department of Aerospace Engineering, University of Michigan, Ann Arbor, MI 48109 USA (e-mail: judepark@umich.edu; ilya@umich.edu).

J. Sun is with the Department of Naval Architecture and Marine Engineering, University of Michigan, Ann Arbor, MI 48109 USA (e-mail: jingsun@umich.edu).

S. Pekarek and R. DeCarlo are with the School of Electrical and Computer Engineering, Purdue University, West Lafayette, IN 47907 USA (e-mail: spekarek@purdue.edu; decarlo@purdue.edu).

P. Stone is with GE Energy Power Conversion Naval Systems, Inc., Pittsburgh, PA 15238 USA (e-mail: philip.stone@ge.com).

D. Opila was with GE Energy Power Conversion Naval Systems, Inc., Pittsburgh, PA 15238 USA. He is now with the Department of Electrical and Computer Engineering, United States Naval Academy, Annapolis, MD 21402 USA (e-mail: opila@usna.edu).

R. Meyer is with the School of Mechanical Engineering, Purdue University, West Lafayette, IN 47907 USA (e-mail: rtmeyer@purdue.edu).

Color versions of one or more of the figures in this paper are available online at http://ieeexplore.ieee.org.

Digital Object Identifier 10.1109/TCST.2015.2402233

the high-power electrical load as an unknown disturbance to the shipboard power system. The PMC is developed in a real-time optimization framework where a cost function is formulated and minimized while constraints that reflect design objectives and operational limitations are enforced. The PMC design, which aims to meet load demands, save fuel, extend generator life cycle, and assure the power quality of the shipboard microgrid, is formulated as a nonlinear model predictive control (NMPC) problem with constraints.

Model predictive control (MPC) is an effective control methodology that exploits the solution of a receding horizon optimal control problem to enforce constraints, such as the operational limits of the IPS, and to shape its transient response [10]–[12]. The ability to solve this optimal control problem in real time, i.e., within one sampling period, is, however, a key requirement for shipboard power management systems. This real-time requirement is very challenging as the system dynamics are fast and the sampling period in these applications is in the order of milliseconds. As in [13] and [14], the time and effort required for on-board NMPC computations need to be reduced as much as possible. The inability to complete the computations of NMPC law in real time can result in loss of stability and degraded performance. Without assured real-time capability, it is also impossible to certify and use such a controller in safety critical applications such as the shipboard power management. Efficient numerical algorithms have been proposed to address challenges in the real-time implementation of MPC.

Diehl *et al.* [15] and Cannon [16] provide an overview of efficient numerical methods and algorithms that have been developed for NMPC. Several algorithms, such as the nonlinear real-time iteration scheme [17]–[20], the Newton-type solver [21], and the continuation and generalized minimum residual [22], have a common feature that they perform one iteration of root finding in each sampling period. The accuracy of finding the solution may, however, be insufficient, and the performance may be degraded for systems with significant nonlinearities. The advanced step algorithm [23] performs a complete Newton-type interior point procedure to convergence to avoid the potential issues associated with the early termination approaches. In [24], the feasibility-perturbed sequential quadratic programming (FP-SQP) algorithm has been proposed. To reduce the computation time, the FP-SQP algorithm maintains all intermediate iterations feasible and exploits suboptimal solutions.

In this paper, we explore the integrated perturbation analysis and SQP (IPA-SQP) framework to develop a PMC. The IPA-SQP approach, developed for NMPC in [25]–[27], combines solution updates derived using perturbation analysis (PA) and SQP. For PA-based update, IPA-SQP exploits neighboring extremal (NE) optimal control theory extended to discrete-time systems with constraints [28] to improve computational efficiency. The solution at time t is obtained as a correction to the solution at time $(t-1)$ through the NE update. If the NE update is not fulfilling optimality criteria, one or multiple SQP updates are exploited until the optimality criteria are satisfied. The merged PA and SQP updates yield a fast solver for NMPC problems [29]. The IPA-SQP algorithm is based on the optimal control and NE theory, which results in efficient updates that are based on backward-in-time solution to discrete-time Riccati equations. Alternative methods based on the sensitivity of the underlying nonlinear programming problem [30]–[32] can also be exploited. The comparison between various approaches is beyond the scope of this paper and is left to future work.

In this paper, we report the results of applying the IPA-SQP algorithm to solve the real-time MPC problem for shipboard PMC. Toward this end, a simplified optimization-oriented design model is derived by approximating components of the transient power management model (TPMM) [33], which is a low-order simulation model of the test bed at Purdue University. We then develop the IPA-SQP-based MPC controller and analyze the performance using the TPMM as the virtual test bed through both nonreal-time and real-time simulations. Finally, the algorithm is implemented on the physical test bed to evaluate its performance in several proposed operational scenarios. The capability to perform the computations in real time, satisfy constraints, and tune the performance attributes is demonstrated.

This paper is organized as follows. In Section II, the shipboard power system and its control objectives are described, and the simulation model is introduced. The optimization-oriented design model of the TPMM is derived by approximation and model order reduction. Then, the MPC problem with constraints is formulated considering various PMC operational requirements and constraints. In Section III, the features of the IPA-SQP-based MPC are reviewed and the algorithm of the IPA-SQP is described. Test scenarios of the proposed PMC for simulations and experiments are discussed in Section IV. The simulation results with the TPMM serving as the virtual test bed on a real-time simulator are reported and analyzed. The experimental results on the physical test bed are presented, analyzed, and compared with the simulation results. Section V ends this paper with the conclusion.

II. System Description and MPC Formulation

A. System Description

The notional power system considered in this paper represents a scaled-down version of a real shipboard power system. It consists of two power generation systems, a ship propulsion motor, and a square-wave pulse power load (SWPPL). This system was developed at Purdue University as an outcome of a sponsored project by the Office of Naval Research [33], and has been used for several sponsored research projects [33], [34]. The schematic of the system is shown in Fig. 1, and the physical appearance of the test bed is shown in Fig. 2.

Generation system 1 (GS-1) is the main shipboard power source and represents a gas turbine generator. Generation system 2 (GS-2) represents a smaller ship power generation source, such as a diesel generator. The SPS is the primary load on the power system. The SWPPL represents the load of an electromagnetic rail gun. The power sources and loads are

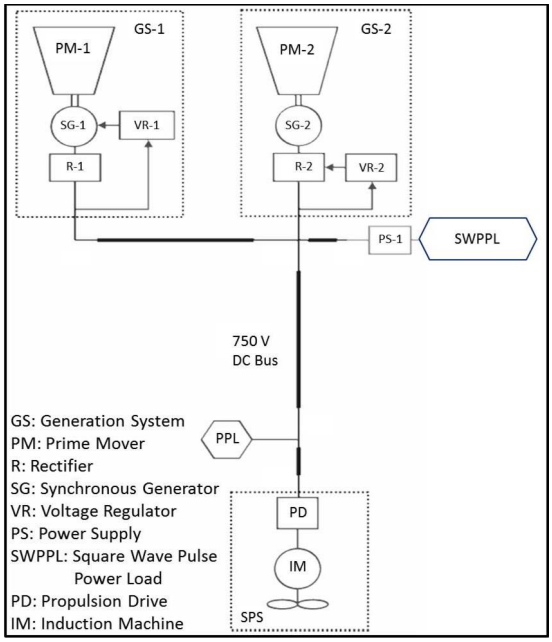

Fig. 1. Schematic of the shipboard power system.

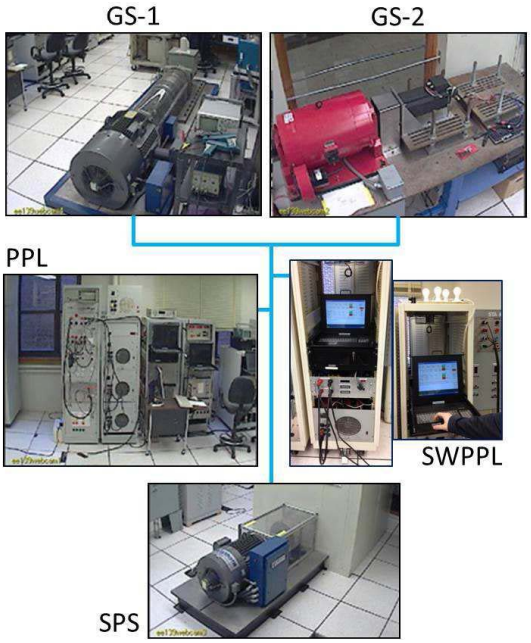

Fig. 2. Physical test bed.

connected in parallel to a 750 V dc bus. The key components and their operational parameters are listed in Table I.

B. Operational Requirements and Control Objectives

For the investigation reported in this paper, we make the following assumptions that are representative of the physical system in the test bed.

1) The desired ship velocity, the SPS induction machine (IM) power and desired speed, and the target bus voltage are constant.
2) The GS-2 operates in the generation mode, has its best efficiency at 5 kW, and has a constant rotor speed.

TABLE I
SUBSYSTEMS OF THE TEST BED

Subsystems	Description	Key operational parameters
GS-1	Prime mover 1 Wound rotor synchronous machine	1800 rpm max. 59 *kW*
GS-2	Prime mover 2 Permanent magnet synchronous machine	3600 rpm max. 11 *kW*
SPS	Propulsion drive Induction machine	1800 rpm max. 37 *kW*
SWPPL	High power buck converter	peak 8 *kW* average 4 *kW*

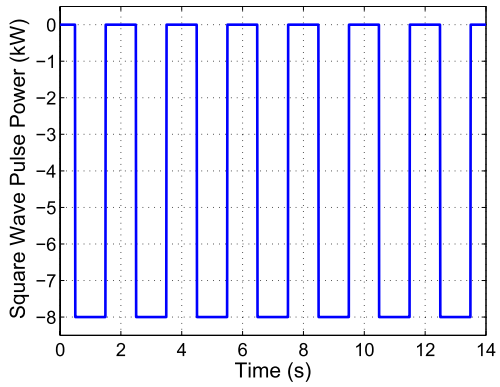

Fig. 3. SWPPL on the TPMM. The pulse starts at 0.5 s with 8-kW amplitude and 1-s duration. The period is 2 s.

3) The pulsed power load consists of square-wave pulses with 8-kW amplitude and 1-s duration (Fig. 3).
4) The PMC has no prior knowledge of the SWPPL, i.e., the SWPPL is an unknown disturbance.
5) The line losses are negligible.

Note that the above-listed assumptions are made to simplify the exposition of the algorithm or to reflect the hardware limitations (such as assumption 3). They can be removed or modified without changing the nature of the problem and the proposed solution. The control objectives of the PMC are to coordinate the power generation sources to meet the load demand and to achieve the following performance attributes:

1) tracking the set points of bus voltage, GS-2 electrical power, SPS electrical power, and SPS rotor speed;
2) protecting and extending the life span of the machines GS-1, GS-2, and SPS;
3) maintaining power quality of the microgrid and minimizing bus voltage variation.

We note that the GS-1 is expected to provide most of the power for SWPPL, which may cause extreme ramping in GS-1 power output due to the set-point tracking objective on GS-2 electrical power and, consequently, have negative impact on the gas turbine and generator life span. Therefore, some of the control objectives are competing with each other and need to be balanced by the PMC system.

C. Optimization-Oriented Design Model and Operational Constraints

The TPMM is a low-order simulation model of the physical test bed that has been established by Purdue University.

TABLE II
STATE VARIABLES, CONTROL INPUTS, AND PARAMETERS IN THE OPTIMIZATION-ORIENTED DESIGN MODEL

Variable	Symbol	Description
State variables	x_1	GS-1 electrical power (kW)
	x_2	IM rotor speed in the SPS (rad/s)
	x_3	DC bus voltage (V)
Control inputs	u_1	GS-1 droop gain
	u_2	GS-2 mechanical power command (kW)
	u_3	SPS mechanical power command (kW)
Parameters	T_s	Sampling time interval (s)
	ω_d	Desired rotor speed of the IM (rpm)
	V_b	Desired bus voltage (V)

It represents the essential dynamics of the power system developed in [33]. Even though the TPMM is already simplified to enable fast simulation, it is still complex to be used for the IPA-SQP algorithm implementation.

The optimization-oriented design model that supports analytical derivations for the IPA-SQP algorithm implementation is developed by simplifying the TPMM model. This model is represented by the following nonlinear discrete-time equations:

$$\begin{aligned} x_1(k+1) &= f_1(x(k),u(k)) \\ &= x_1(k) + \frac{T_s x_3(k+1)}{x_3(k+1)+c_1u_1(k)}z(k) \quad (1)\\ x_2(k+1) &= f_2(x(k),u(k)) \\ &= \frac{1}{1+T_sc_2c_3}(x_2(k)+T_sc_2(c_3\omega_d+c_4u_3(k))) \quad (2)\\ x_3(k+1) &= f_3(x(k),u(k)) \\ &= \frac{1}{1+T_sc_5}\left(x_3(k)+T_s\sqrt{c_6x_3^2(k)+c_7P_s(k)}\right) \quad (3)\end{aligned}$$

where

$$\begin{aligned} x(k) &= (x_1(k)\ \ x_2(k)\ \ x_3(k))^T \\ u(k) &= (u_1(k)\ \ u_2(k)\ \ u_3(k))^T \\ z(k) &= c_1\left(\frac{u_1(k)x_1(k)}{x_3^2(k+1)}-1\right) \\ &\quad\times\left(-c_5x_3(k+1)+\sqrt{c_6x_3^2(k)+c_7P_s(k)}\right) \\ &\quad+c_8(V_b-x_3(k))-\frac{c_8u_1(k)x_1(k)}{x_3(k+1)} \\ P_2(k) &= c_9u_2^2(k)+c_{10}u_2(k) \\ P_3(k) &= (c_{11}+c_{12}x_2(k))u_3(k) \\ P_s(k) &= x_1(k)+P_2(k)+P_3(k)+P_4(k). \end{aligned}$$

Equations (1)–(3) are derived from the TPMM model based on several simplifying assumptions and approximations [33] and discretized using the backward Euler method. Table II summarizes the state variables, the control inputs, and parameters in (1)–(3). The droop gain u_1 of the voltage controller in the GS-1 is a control input. This GS-1 droop gain impacts the dc bus voltage. It is used to indirectly control the output power of the GS-1. The GS-2 and SPS receive the GS-2 and SPS mechanical power commands from the PMC, respectively. Then, their inner loop controllers convert the power commands to torque commands and current commands to accomplish tracking of these power commands using hysteresis control [33]. $P_2(k)$ and $P_3(k)$ are the GS-2 and SPS electrical power, respectively, and $P_4(k)$ is the square-wave pulse power at sampling instant k. $P_s(k)$ is the sum of the GS-1, GS-2, SPS electrical power, and the SWPPL power at sampling instant k. These values are required to estimate GS-2 electrical power, SPS electrical power, the SWPPL power, and the sum of the electrical power with the state variables and control inputs at sampling instant k. The parameters $c_i,\ i=1,\ldots,12$, are constants used in the equations [33]. Positive sign is used for electrical power generated, and negative sign is used for electrical power consumed.

The system has several constraints that represent hardware limitations and operational requirements. The GS-1, GS-2, and SPS have operational limitations of 59, 11, and 37 kW, respectively, as given in Table I. The GS-1 droop gain takes values in the interval $[-1,\ 1]$. The constraints are mathematically expressed as

$$0 \le x_1(k) \le 59 \quad (4)$$
$$-1 \le u_1(k) \le 1 \quad (5)$$
$$-11 \le u_2(k) \le 0 \quad (6)$$
$$0 \le u_3(k) \le 37. \quad (7)$$

Note that the system is nonlinear with constraints that include a pure state constraint (4) and pure control constraints (5)–(7). Since the model is nonlinear, the NMPC approach is pursued to provide reconfigurability to changing model parameters, requirements, and faults.

D. MPC Problem Formulation

The MPC problem is formulated by considering the control objectives and operational assumptions

$$\min_{\substack{x(\cdot)\in\mathbb{R}^3,\\ u(\cdot)\in\mathbb{R}^3}} J(x(\cdot),u(\cdot)) \quad (8)$$

where

$$J(x(\cdot),u(\cdot)) = \Phi(x(t+N)) + \sum_{k=t}^{t+N-1} L(x(k),u(k)) \quad (9)$$

and

$$\begin{aligned} L(x(k),u(k)) &= k_1(x_3(k)-V_b)^2 + k_2(P_2(k)-P_{2d})^2 \\ &\quad + k_3(P_3(k)-P_{3d})^2 + k_4(x_2(k)-\omega_d)^2 \\ &\quad + k_5(u_1(k)-u_1(k-1))^2 \\ &\quad + k_6(x_1(k)-x_1(k-1))^2 \\ &\quad + k_7(P_2(k)-P_2(k-1))^2 \\ &\quad + k_8(P_3(k)-P_3(k-1))^2 \\ \Phi(x(t+N)) &= \phi_1(x_2(t+N)-\omega_d)^2 + \phi_2(x_3(t+N)-V_b)^2 \end{aligned}$$

for all $k\in[t,\ t+N-1]$, subject to (1)–(3) and (4)–(7).

Here, P_{2d} and P_{3d} are the desired GS-2 electrical power and the desired SPS electrical power, respectively. x_t is the state at a sampling instant t. $k_j,\ j=1,\ldots,8$, denote weighting factors on different terms in the cost function.

TABLE III
WEIGHTING FACTORS IN THE COST FUNCTION ON THE TEST BED

Physical meaning on the test bed	Weight	Test A (Baseline)	Test B (Increase k_6)	Test C (Increase k_3)
DC bus voltage deviation	k_1	1	1	1
GS-2 power deviation	k_2	15	15	15
SPS power deviation	k_3	15	15	**25**
SPS induction machine speed deviation	k_4	1	1	1
Ramp rate of GS-1 droop gain	k_5	13	13	13
Ramp rate of GS-1 power	k_6	1	**10**	**10**
Ramp rate of GS-2 power	k_7	0.1	0.1	0.1
Ramp rate of SPS power	k_8	0.1	0.1	0.1
SPS induction machine speed deviation	ϕ_1	100	100	100
DC bus voltage deviation	ϕ_2	100	100	100

Each weighting factor k_j assigns a relative priority to a performance aspect. The first term in $L(x(k), u(k))$, the error between the measured bus voltage and the desired bus voltage, is related to bus voltage tracking. Minimizing this error helps assure power quality on the microgrid. The second term is for GS-2 to operate at the most efficient point. The other terms reflect SPS electrical power tracking of the desired value, SPS rotor speed tracking for maintaining the desired ship velocity, droop gain ramp rate, GS-1 electrical power ramp rate, GS-2 electrical power ramp rate, and SPS electrical power ramp rate. Component wear is reduced by penalizing power ramp rate. The $\Phi(x(t+N))$ is the terminal cost function to penalize the deviation of $x_2(t+N)$ and $x_3(t+N)$ from their desired values with weighting factors of ϕ_1 and ϕ_2, respectively. The GS-1 is treated as a slack generator and provides the power necessary to balance the generating power and consumed power. Hence, $x_1(k)$ is not penalized. The values of the weighting factors used for the cost function are listed in Table III.

Solving the MPC problem (8) subject to the constraints in real time requires an effective optimization algorithm. The IPA-SQP algorithm, which has been shown to have advantages in computational efficiency for NMPC [29], is reviewed in Section III.

III. OVERVIEW OF IPA-SQP ALGORITHM

The IPA-SQP algorithm combines the complementary features of PA and SQP for solving constrained dynamic optimization problems [26], [27], [35], [37]. PA is an approach to predict a change in the optimal solution when some of the parameters, such as the initial conditions, are changed. The PA provides closed-form solutions and makes the optimization computationally efficient. Because of the approximate nature of the PA solution, however, it does not guarantee successive optimality when the algorithm is applied repeatedly to update a nominal solution. To correct the solution so that it satisfies the necessary conditions to a specified tolerance, an SQP update based on linearization and quadratic cost approximation can be applied. Through synergetic integration of these two algorithms, the optimal control sequence at each sampling instant t with the observed state $x(t)$ is calculated using the optimal control sequence from the previous sampling instant $(t-1)$. It can be shown that the IPA-SQP has a linear computational complexity of $O(N)$ as compared with SQP that has complexity from $O(N^{1.5})$ to $O(N^3)$, where N is the prediction horizon of the MPC problem [29]. Moreover, the IPA-SQP has the following features.

1) The IPA-SQP efficiently computes the approximation of the optimal solution by taking advantage of backward-in-time recursive updates.
2) When active constraints are not changed by the perturbation, $\delta x(t) = x(t) - x(t-1)$, in the initial state, the closed-form PA solution can be derived, thereby leading to a very efficient computation. If the variation $\delta x(t)$ in the initial state causes changes in the activity status of constraints, the variation $\delta x(t)$ is divided into smaller segments so that the PA solution can be applied to each of these segments to sequentially update the solution. It has been shown in several applications that a good tradeoff between efficient computation and accurate optimization can be achieved [25], [27], [37].

Let C and $\bar{C}$ denote the mixed state-input constraints and pure state constraints

$$C = \begin{pmatrix} -u_1 - 1 \\ u_1 - 1 \\ -u_2 - 11 \\ u_2 \\ -u_3 \\ u_3 - 37 \end{pmatrix}, \quad \bar{C} = \begin{pmatrix} -x_1 \\ x_1 - 59 \end{pmatrix}. \tag{10}$$

The IPA-SQP algorithm computes the new control sequence over the prediction horizon in the form of

$$u^{(i+1)}(k) = u^{(i)}(k) + \delta u^{(i)}(k) \tag{11}$$

where $k \in [t, t+N]$, $\delta u^{(i)}(k)$ is given by

$$\delta u^{(i)}(k) = -(I \quad 0) K_0(k) \times \begin{pmatrix} Z_{21}(k)\delta x^{(i)}(k) + f_u(k)^T T(k+1) + H_u(k) \\ \tilde{C}_x^a(k)\delta x^{(i)}(k) \end{pmatrix} \tag{12}$$

and i is the iteration index. For $i = 0$, $u^{(0)}(k)$ is taken as the solution sequence calculated at the previous sampling instant $(t-1)$. The matrices K_0, Z_{21}, $\tilde{C}_x^a$, and T are defined by the IPA-SQP algorithm. The detailed calculation steps are

given in the Appendix. H_u and f_u are the partial derivatives of the Hamiltonian function (13) and of the right-hand side of (1)–(3), i.e., $f(k) = (f_1(k)\ f_2(k)\ f_3(k))^T$ with respect to u, evaluated at $u^{(i)}(k)$, respectively. Note that the predictor update is integrated with a corrector update that accounts for nonzero H_u. In the IPA-SQP algorithm, we terminate the iterations if $\sum_{k=t}^{t+N-1} |H_u(k)| < H_u^t$ for some small threshold H_u^t. A good tradeoff can be achieved between efficient computation and accuracy of the optimization by properly selecting H_u^t, for instance, [38] where the tradeoff between computation time and optimality is illustrated for a spacecraft relative motion control problem in which the impact of different termination thresholds is evaluated. In this paper, H_u^t was chosen as 0.01 both in the simulations and experiments. Several iterations may be needed to satisfy the criterion $\sum_{k=t}^{t+N-1} |H_u(k)| < H_u^t$.

The algorithm realization is based on a combination of a MATLAB script function and some Simulink blocks from the standard Simulink library. Fig. 4 shows the key steps of the IPA-SQP algorithm in the form of a pseudocode.

Measure $x(t)$ and let
$x(t-1)$ and the nominal solution sequences $x^*(\cdot)$, $u^*(\cdot)$ be given from the previous time instant $(t-1)$.
1. Initialization:
Set $i = 0$, $\delta x^{(i)}(t) = x(t) - x(t-1)$, $x^{(i)}(\cdot) = x^*(\cdot)$, and $u^{(i)}(\cdot) = u^*(\cdot)$.
2. Evaluate the matrices $Z_{11}(k)$, $Z_{21}(k)$, $Z_{22}(k)$, $K_0(k)$, $S(k)$, and $T(k)$ for $k = t, \ldots, t+N-1$ according to equation (28).
Calculate $\delta u^{(i)}(k)$ by equation (12).
3. Find the smallest α_i among $\alpha_{ik} \in [0, 1]$ such that the perturbation $\alpha_i \delta x^{(i)}(k)$ changes the status of the constraint at least at one instant. (See [26] for details.)
4.
if $\alpha_i = 1$ **then**
  Set $u^{(i+1)}(\cdot) = u^{(i)}(\cdot) + \delta u^{(i)}(\cdot)$,
  $x^{(i+1)}(\cdot) = x^{(i)}(\cdot) + \delta x^{(i)}(\cdot)$,
  if $\sum_{k=t}^{t+N-1} |H_u(k)| < H_u^t$ **then**
    Obtain an optimal solution $u^{(i+1)}(\cdot)$ and $x^{(i+1)}(\cdot)$.
  else
    Set $\delta x^{(i+1)} = 0$ and $i = i + 1$ for SQP updates.
    Go to step 2.
  end
else
  if $0 < \alpha_i < 1$ **then**
    Set $u^{(i+1)}(\cdot) = u^{(i)}(\cdot) + \alpha_i \delta u^{(i)}(\cdot)$,
    $x^{(i+1)}(\cdot) = x^{(i)}(\cdot) + \alpha_i \delta x^{(i)}(\cdot)$,
    and
    $\delta x^{(i+1)}(\cdot) = (1 - \alpha_i)\delta x^{(i)}(\cdot)$,
    $i = i + 1$.
    Go to step 2.
  else
    $\alpha_i = 0$.
    Change the activity status of the corresponding constraint.
    Go to step 2.
  end
end

Fig. 4. Illustration of the IPA-SQP algorithm.

IV. Simulation and Experimental Results

The power management strategy using MPC, where the optimization of (8) subject to (4)–(7) is solved using the IPA-SQP algorithm at each sampling period, has been tested via simulations and experiments. We note that after the initial design and simulation analysis, high sensitivity of control performance to uncertainty in SWPPL delivery timing was identified, i.e., when the SWPPL is treated as a known disturbance, the performance of the PMC varied if the actual ON and OFF times for SWPPL are different from the assumed values. It was decided that the SWPPL will be treated as an unknown disturbance.

The design and implementation of MPC based on the IPA-SQP approach has been performed first in the simulation environment using the TPMM, then in the Opal-RT real-time simulator, and, finally, on the Purdue physical test bed. The design and implementation process is shown in Fig. 5.

Given the hardware limitations of the test bed, we consider the SWPPL waveform shown in Fig. 3, which sinks up to 8 kW for 1-s intervals over seven consecutive cycles. The reference set points for tracking are $P_{2d} = 5$ kW, $P_{3d} = -10$ kW, and $V_b = 750$ V for GS-2 electrical power, SPS electrical power, and bus voltage, respectively, in simulations and experiments. The prediction horizon is chosen as five sample intervals, and the sampling time interval is set to 20 ms to balance the algorithm execution time with the prediction horizon duration. Hence, the PMC is able to look ahead 0.1 s.

The PMC metrics are developed to evaluate and quantify the performance of the PMC using the IPA-SQP-based MPC. The metrics reflect: 1) load-following performance measured by maximum and average deviation of SPS power from its set point; 2) fuel efficiency in terms of deviation of GS-2 from its optimal setting; 3) power quality represented by bus voltage deviation from 750 V; and 4) gas turbine machinery protection in terms of the maximum and average absolute ramp rate of GS-1 and operating time interval when the ramp rate exceeds a certain threshold. The value of absolute GS-1 ramp rate threshold is chosen to be slightly lower than the maximum absolute GS-1 ramp rate (90 kW/s in simulations and 35 kW/s in experiments) to measure the duration that the absolute GS-1 ramp rate exceeds the threshold as a bad baseline.

A. Effects of Computational Delay

For the PMC problem described in Section II, the performance will depend on the choice of the parameters in the cost function (9). Computational delays can also have a significant impact on system performance. To demonstrate the effects of delays, simulations were performed using the TPMM as the plant and the MPC as the controller.

We assume 30-ms computational delay when evaluating its effects on performance. With 20-ms sampling time, this will lead to an overrun in real time. This overrun has two consequences: 1) the delay in the control execution and 2) the

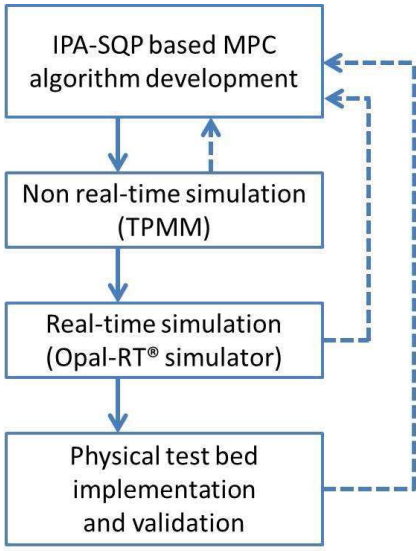

Fig. 5. Design and implementation procedure of the IPA-SQP-based MPC approach.

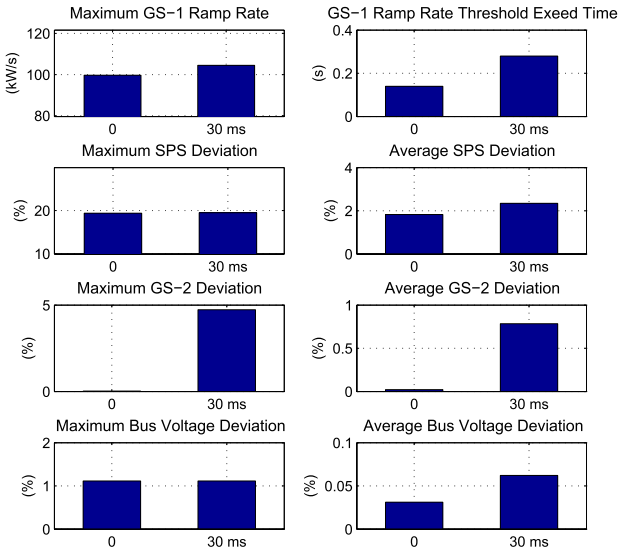

Fig. 6. Performance analysis with 30-ms computational time delay on the TPMM.

effective loss of the sampling rate, since the system cannot respond to the next immediate sample data before it completes the current computation. These effects have been modeled in simulations, and the results are shown in Fig. 6.

As shown in Fig. 6, performance degradation, in terms of those four metrics defined for the shipboard PMC, is noticeable. The results highlight the performance degradation with the delay and the importance of computationally efficient MPC implementation that aims at minimizing the computational delay.

B. Case Study Scenarios

The effectiveness of the optimization-based PMC strategy is examined with emphasis being placed on different ship performance attributes, such as protecting the main generator GS-1 and extending its life span through reduced GS-1 ramp rate, and improving SPS tracking performance. Among many available paths, several scenarios are designed to test the PMC algorithm and to evaluate the performance as well as the sensitivity to key design parameters and tunability of the controller.

1) Test A characterizes the baseline performance. After closing the control loop between the PMC and the test bed, the weighting factors are tuned to meet different objectives by running many simulations. The weighting factors for the baseline were selected as shown in Table III.
2) Test B reflects the performance of the PMC algorithm when protecting the GS-1 is emphasized, where the penalty k_6 on the ramp rate of GS-1 is increased (from 1 to 10).
3) Test C examines how the SPS tracking performance can be improved after the SPS response is compromised in Test B as a consequence of relaxed control authority in GS-1. The new GS-1 ramp rate of Test B is maintained, and the penalty k_3 on the SPS IM power is increased (from 15 to 25).

The weighting factors for each scenario are reported in Table III.

C. Numerical Simulation Results

Simulations are performed for the three scenarios using the TPMM as the plant model. The results are shown in Fig. 7. Plots present only one pulse period to avoid repetition since the results for other pulses are identical. Fig. 8 summarizes the performance metrics obtained from TPMM simulations. Note that in Fig. 7, all set-point tracking objectives are achieved with high accuracy (within 1% for GS-2 electrical power, 2% for SPS electrical power, and 0.05% for bus voltage in average root-mean-square deviation from the desired values). The square-wave load demand is also met with fast response time in all three scenarios.

The maximum absolute GS-1 ramp rate is essentially unchanged from Test A to Test B, as shown in Fig. 8, while the average value of GS-1 ramp rate reduces 4.5% as the penalty on GS-1 ramp rate increases, as summarized in Table IV. Given that the SWPPL is treated as an unknown disturbance, the maximum ramp rate always occurs when the pulse rises. As side effects, SPS and GS-2 electrical power tracking errors increase, namely, SPS and GS-2 electrical power tracking performances are sacrificed in Test B. To mitigate some of these effects, the penalty on SPS tracking error is increased from Test B to C. There are several consequences of increasing k_4. First, SPS tracking error is decreased. Second, the average value of GS-1 ramp rate is increased slightly (but still less than that in Test A). Finally, GS-2 electrical power tracking error is increased in Test C from Test B while SPS tracking is improved. The bus voltage tracking behavior correlates to the change in the average value of GS-1 ramp rate. Table IV also reports the time intervals when GS-1 ramp rate exceeds a threshold of 90 kW/s. GS-1 ramp rate that exceeds 90 kW/s occurs less frequently in the simulation for 14 s in Tests B and C.

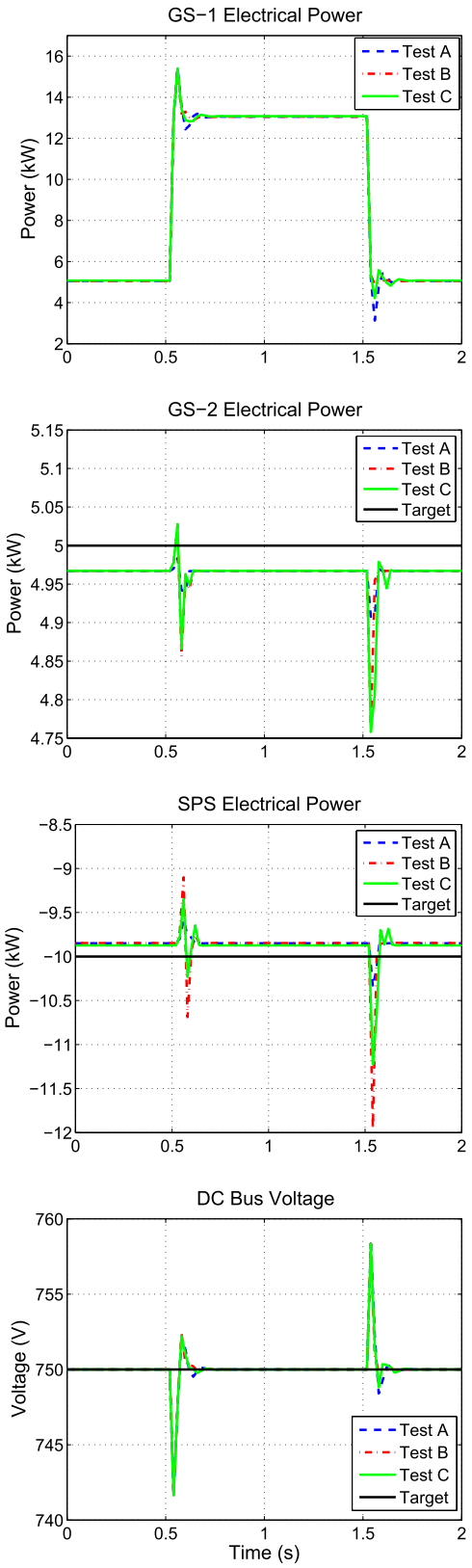

Fig. 7. Responses on the TPMM. From top to bottom: GS-1 electrical power, GS-2 electrical power, SPS electrical power, and dc bus voltage.

The simulation results show that the IPA-SQP algorithm can be used effectively for power management to balance different objectives. They also illustrate that, through adjustment of different weighting factors in the cost function, one can emphasize different aspects of the performance attributes and achieve the desired tuning of the controller performance.

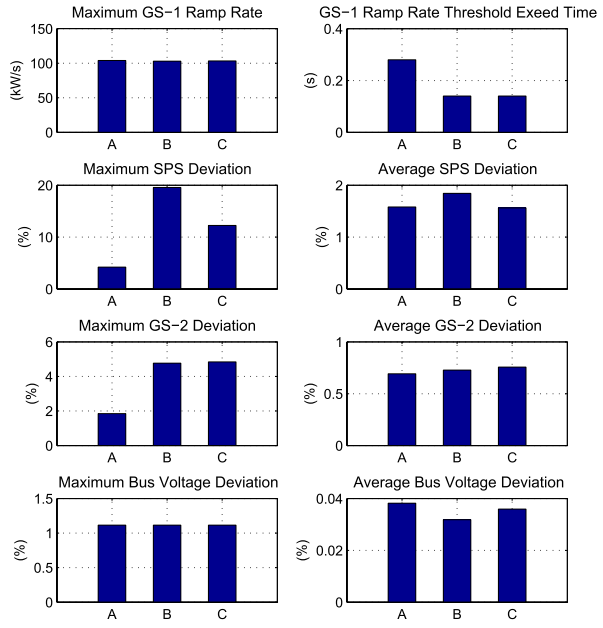

Fig. 8. Performance analysis on the TPMM.

TABLE IV
PMC SIMULATION METRICS ON THE TPMM

Test	Average GS-1 ramp rate (kW/s)	GS-1 ramp rate threshold exceed time out of 14 seconds (s)
A	9.05	0.28
B	8.64	0.14
C	8.84	0.14

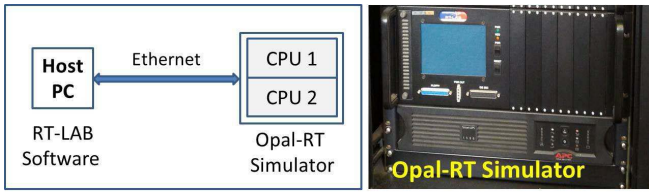

Fig. 9. Real-time simulation system. (a) System configuration. (b) Opal-RT simulator.

D. Real-Time Simulation Results

Before implementing the IPA-SQP algorithm on the physical test bed, we run real-time simulations on an Opal-RT simulator to verify the feasibility of real-time implementation of our MPC algorithm and assess its performance.

The RT-LAB system is used to implement the real-time simulations. The real-time simulation setup is shown in Fig. 9. The RT-LAB system includes a host personal computer (PC) and an Opal-RT simulator as a PC cluster-based platform. The simulator has two CPUs that can exchange information through the shared memory. The host PC and the simulator can communicate via the Ethernet connection with 1-Gbit/s speed.

TABLE V
WORST CASE COMPUTATION TIME ON THE Opal-RT SIMULATOR

Prediction horizon	5 (0.1 sec)	25 (0.5 sec)	50 (1 sec)
Computation time	1.5 *ms*	6 *ms*	12 *ms*

Through real-time simulations on the Opal-RT simulator, we check for overruns, algorithm execution time, and feasibility of real-time implementation.

The waveform responses, tracking performance, and execution time are evaluated to assess the real-time behavior of the proposed IPA-SQP solution. The same SWPPL power profile in Fig. 3 and the same test scenarios are considered. The TPMM model is used as the virtual plant and simulated with the PMC.

Fig. 10 shows the profiles of the number of SQP iterations, the value of optimality criterion $\sum_{k=t}^{t+N-1} |H_u(k)|$, and the value of the objective function for all scenarios. The maximum number of SQP iterations is set to 10. One can observe that a single SQP iteration was sufficient at 93% of the time instants for the one square-wave period run. When large reference changes happened (i.e., at 0.5 and 1.5 s), the number of iterations, the value of optimality criterion, and the value of the cost function all increased, due to the fact that the SQP iteration limit was reached and the IPA-SQP algorithm was terminated before achieving optimality.

Fig. 11 shows the waveform responses in real-time simulation and compares them with nonreal-time simulation of the one square-wave period run for Test A. Both cases have the identical responses, demonstrating that there are no overruns in real-time simulation. Table V summarizes the worst case measured computation time on the real-time simulator with the same solver settings as the prediction horizon length changes. As one can observe from Table V, the computation time grows approximately linearly with respect to the prediction horizon, which is consistent with [29]. The IPA-SQP algorithm is shown to be sufficiently fast for online optimization in this application. Even for the prediction horizon of 50 steps with a sampling time of 20 ms (which corresponds to 1-s prediction window), it takes less than 12 ms to perform the optimization and no overruns have been observed on the Opal-RT simulator.

We note that even though the maximum iteration number was reached and the IPA-SQP terminated the computation without reaching the optimality condition (i.e., at 0.62 and 1.58 s), the IPA-SQP did provide feasible solutions, and those solutions were used as initial guesses for the solution at the next instants. The issue of loss of feasibility was not encountered in our real-time simulation and experiments. In general, however, how to guarantee feasibility in the case of hitting iteration limitation is an important issue, common to many state-of-the-art MPC solvers, which is left to future research.

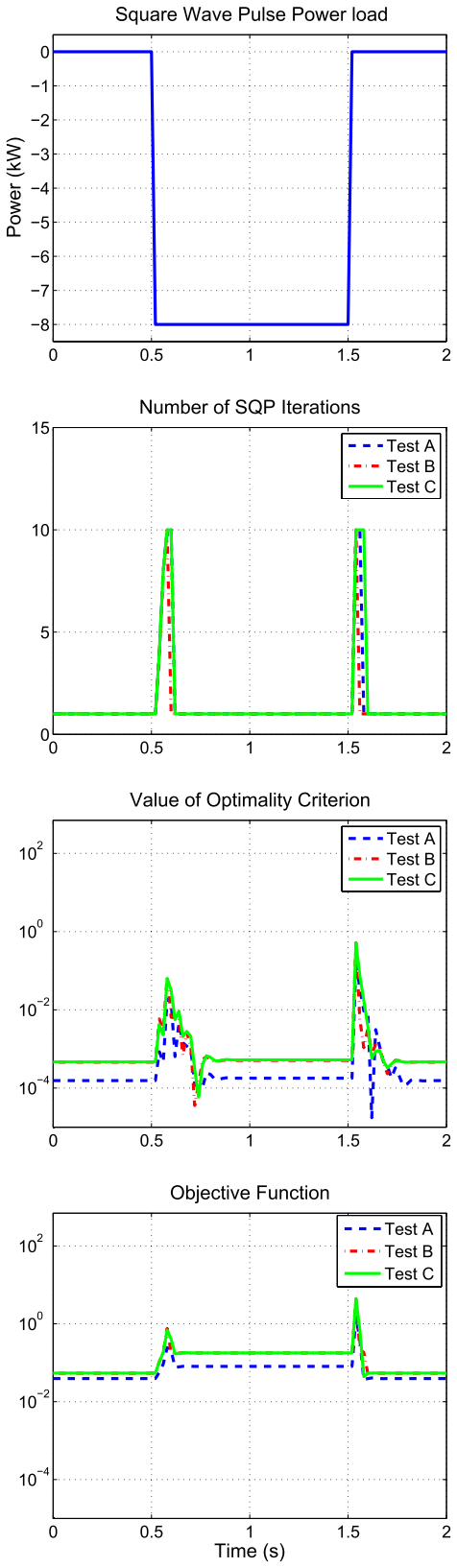

Fig. 10. Responses of real-time simulations. From top to bottom: SWPPL, number of SQP iterations, value of optimality criterion, and value of objective function.

E. Experimental Results on the Purdue Physical Test Bed

In this section, we analyze the experimental results obtained when the algorithm is implemented on the Purdue physical test bed. The SWPPL is shown in Fig. 12, and the same testing scenarios A–C and the same reference set points for tracking used in the simulations are used in the experiments.

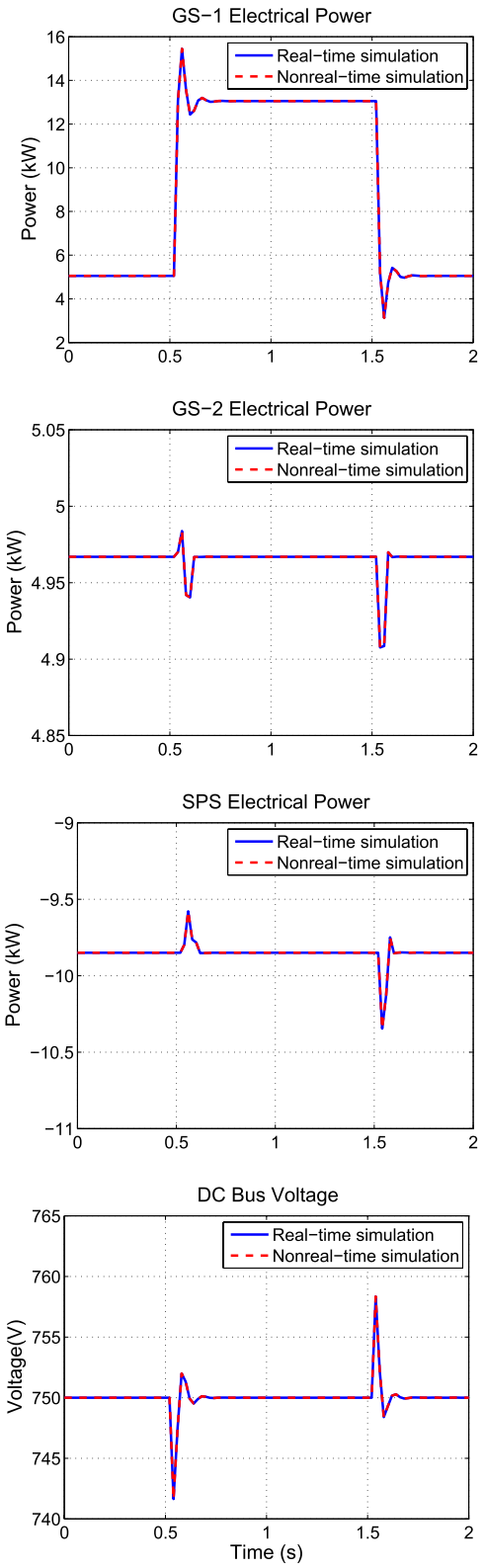

Fig. 11. Responses of real-time simulation and nonreal-time simulation. From top to bottom: GS-1 electrical power, GS-2 electrical power, SPS electrical power, and dc bus voltage.

Fig. 13 presents the control inputs, while Fig. 14 shows the waveform responses (only one pulse period) in Tests A–C. Fig. 15 reports the metrics for the measured values on the

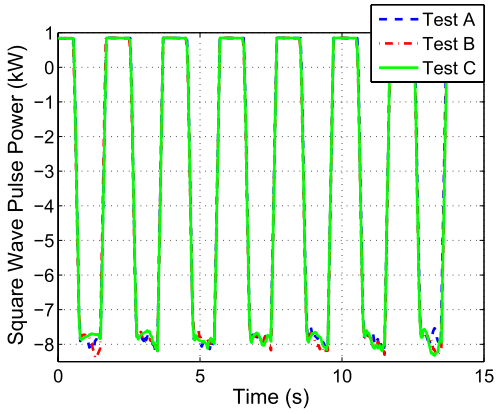

Fig. 12. SWPPL on the physical test bed.

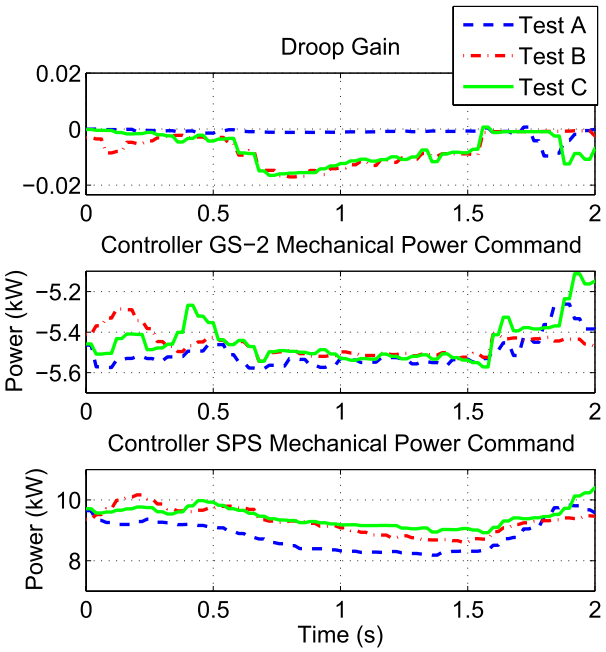

Fig. 13. Control inputs of PMC using IPA-SQP-based MPC on the test bed.

physical test bed. Since the SWPPL is assumed to be unknown, the maximum absolute GS-1 ramp rate occurs when the pulse first rise, and the maximum values are similar in the test cases, as shown in Fig. 15. Table VI shows that the average value of GS-1 ramp rate reduces from Test A to B as the penalty on GS-1 ramp rate increases, confirming the simulation results. As observed in the simulation, SPS and GS-2 power tracking performances are sacrificed, reflected by the increased in the tracking errors for Test B. From Test B to C, the penalty on SPS tracking error is increased to mitigate some of the effects. Similar to the results obtained in the simulations, SPS tracking error is decreased, as shown in Fig. 15, while GS-2 power tracking performance is sacrificed to accommodate SPS power tracking in Test C as compared with Test B.

Table VI reports the maximum GS-1 ramp rate and the time intervals when GS-1 ramp rate exceeds a threshold of 35 kW/s. The maximum ramp rate of GS-1 is over 40 kW/s for all tests. The time intervals when GS-1 ramp rate exceeds the threshold

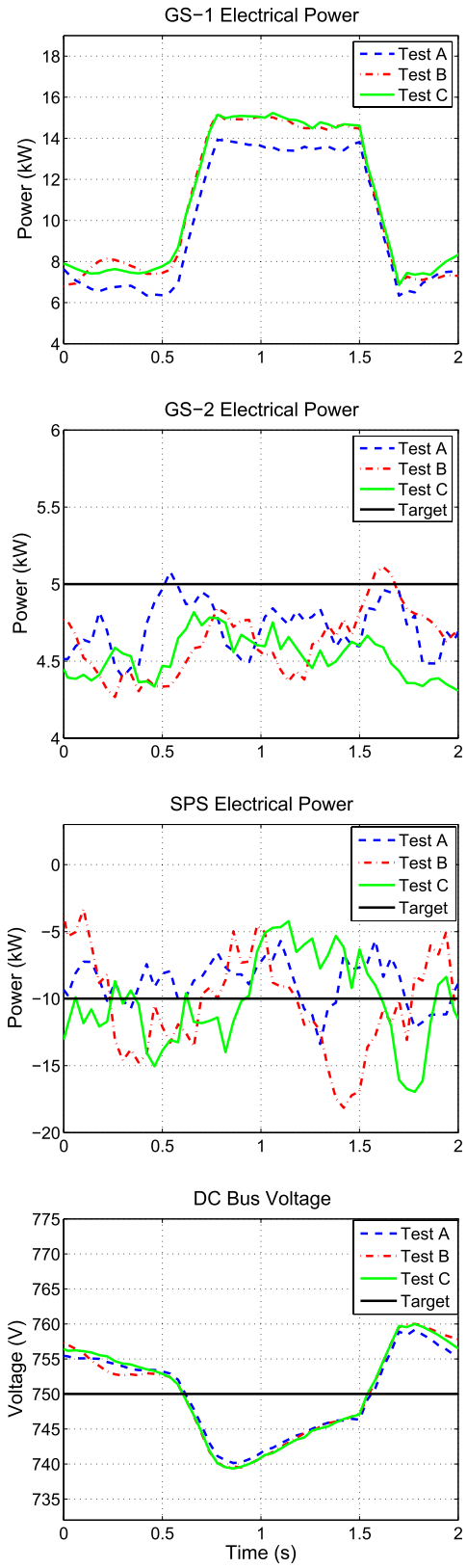

Fig. 14. Responses on the physical test bed. From top to bottom: GS-1 electrical power, GS-2 electrical power, SPS electrical power, and dc bus voltage.

decrease from Test A to B and C, namely, the duration that larger GS-1 ramp rate occurs is less.

The experimental results on the physical test bed are qualitatively correlated to the simulation results. They also

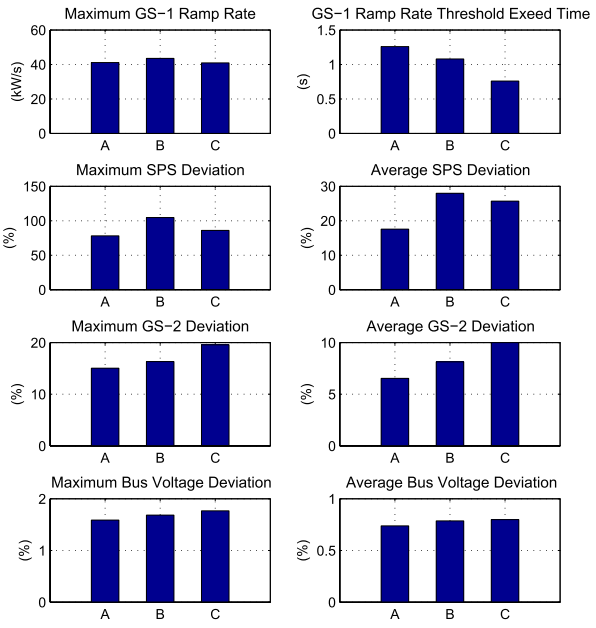

Fig. 15. Performance analysis on the physical test bed.

TABLE VI
PERFORMANCE ANALYSIS OF GS-1 RAMP RATE ON THE TEST BED

Test	Average GS-1 ramp rate (kW/s)	GS-1 ramp rate threshold exceed time out of 14 seconds (s)
A	9.07	1.26
B	8.88	1.08
C	8.45	0.76

experimentally demonstrate the feasibility and performance of the IPA-SQP-based PMC. The differences in the numerical values are attributed to unmodeled physical entities, such as power converters, line losses, as well as unmodeled dynamics of the motors and generators.

V. CONCLUSION

A power management controller for a shipboard power system that uses the IPA-SQP-based MPC has been developed, analyzed, and tested on the simulation model, the Opal-RT real-time simulator, and the physical test bed. The experimental results on the physical test bed and the simulation results are qualitatively correlated. Evaluations of three operational scenarios, Tests A, B, and C, reveal the expected performance sensitivity with respect to tunable parameters, such as the penalties on GS-1 ramp rate and SPS tracking error. The developed PMC successfully allocates requests to power sources and loads in the baseline test with the SWPPL and appropriately modifies control inputs when different aspects of the performance attributes are emphasized by changing weighting factors in the cost function for the MPC problem. This paper demonstrates the feasibility of using the IPA-SQP-based MPC algorithm for real-time power management of shipboard IPS and provides a case that supports further development and implementation of optimization-based PMC for shipboard power systems.

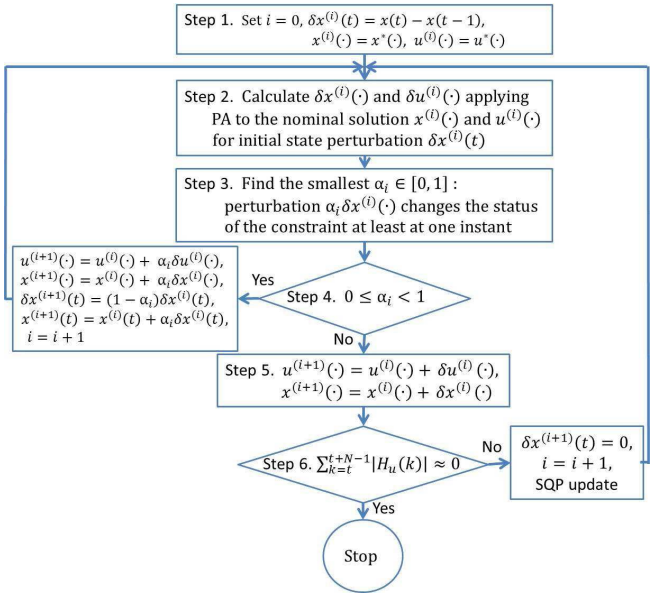

Fig. 16. Flowchart of the IPA-SQP algorithm [37].

APPENDIX
IPA-SQP ALGORITHM

Assume that $(x^*(k),\ u^*(k))$ is the nominal solution to (8). The Hamiltonian function is defined as

$$H(k) = L(x(k),u(k)) + \lambda(k+1)^T f(x(k),u(k)) + \mu(k)^T C^a(x(k),u(k)) + \bar{\mu}(k)^T \bar{C}^a(x(k)) \quad (13)$$

where $\lambda(\cdot)$ is the sequence of costates associated with $f(x(k),u(k))$ (i.e., the dynamics of system), $\mu(k)$ and $\bar{\mu}(k)$ are the vectors of Lagrange multipliers, and $C^a(x(k),u(k))$ and $\bar{C}^a(x(k))$ denote vectors consisting of the active constraints. Before proceeding, we define compact notations for partial derivatives as follows:

$$G_a(k) := \frac{\partial}{\partial a}G(k), \quad G_{ab}(k) := \frac{\partial}{\partial b}\left(\frac{\partial}{\partial a}G(k)\right)$$

where the subscript letters a and b denote the variable G with respect to which the partial derivative is taken, i.e., H_x and H_u denote the partial derivative of H with respect to x and u, respectively.

Since the nominal solution $x^*(\cdot)$ and $u^*(\cdot)$ is optimal, the following necessary optimality conditions are satisfied [36]:

$$\begin{aligned} \lambda(k) &= H_x(k),\ k=t,\dots,t+N-1 \\ H_u(k) &= 0,\ k=t,\dots,t+N-1 \\ \lambda(t+N) &= \Phi_x(x(t+N)) \\ \mu(k) &\ge 0,\ k=t,\dots,t+N-1 \\ \bar{\mu}(k) &\ge 0,\ k=t,\dots,t+N. \end{aligned} \quad (14)$$

The NE solution [28] approximates the optimal state and control sequences for the perturbed initial state so that the necessary conditions (14) for optimality are maintained to the first order.

The flowchart in Fig. 16 shows the main steps to obtain the NE solutions and to deal with changes in the activity status of constraints. The NE solution in Step 2 of the flowchart is obtained by solving the following optimization problem [27], [29], [37]:

$$\min_{\delta x(\cdot),\ \delta u(\cdot)} \delta^2 \bar{J} \quad (15)$$

where

$$\delta^2 \bar{J} = \frac{1}{2}\delta x(t+N)^T \Phi_{11}(t+N)\delta x(t+N) + \frac{1}{2}\sum_{k=t}^{t+N-1} \begin{pmatrix} \delta x(k) \\ \delta u(k) \end{pmatrix}^T \begin{pmatrix} H_{xx}(k) & H_{xu}(k) \\ H_{ux}(k) & H_{uu}(k) \end{pmatrix} \begin{pmatrix} \delta x(k) \\ \delta u(k) \end{pmatrix}$$

$$\text{s.t. } \delta x(k+1) = f_x(k)\delta x(k) + f_u(k)\delta u(k) \quad (16)$$

$$\delta x(t) = \delta x_t \quad (17)$$

$$C_x^a(x(k),u(k))\delta x(k) + C_u^a(x(k),u(k))\delta u(k) = 0 \quad (18)$$

$$\bar{C}_x^a(x(k))\delta x(k) = 0 \quad (19)$$

where δx_t is defined as $\delta x_t := x(t) - x(t-1)$ and $\Phi_{11}(t+N) := \Phi_{xx}(t+N) + (\partial/\partial x)(\bar{C}_x^a(x(t+N))^T \bar{\mu}(t+N))$.

When $C_u^a(k)$ has dependent rows, it can be transformed through linear similarity transformation into the following form:

$$\begin{pmatrix} \tilde{C}_u^a(k) \\ 0 \end{pmatrix} \quad (20)$$

for some $\tilde{C}_u^a(k)$ with independent rows. Hence, (18) is decomposed into

$$\tilde{C}_x^a(x(k),u(k))\delta x(k) + \tilde{C}_u^a(x(k),u(k))\delta u(k) = 0 \quad (21)$$

$$\hat{C}_x^a(x(k))\delta x(k) = 0 \quad (22)$$

for appropriately defined $\tilde{C}_x^a(x(k),u(k))$ and $C_x^a(x(k))$. The independence of the rows in $\tilde{C}_u^a$ is required for NE solution calculation.

We now define matrix sequences $\tilde{C}_u(\cdot)$, $\tilde{C}_x(\cdot)$. $\hat{C}_u(\cdot)$, and $\hat{C}_x(\cdot)$, and $S(\cdot)$ using the following backward recursive equations. Define

$$\hat{C}_x^a(t+N) := \bar{C}_x^a(x(t+N)) \quad (23)$$

$$S(t+N) := \Phi_{11}(t+N) \quad (24)$$

and at sampling instant k, let

$$C_{\text{aug}}(k) := \begin{pmatrix} C_u^a(k) \\ \hat{C}_x^a(k+1)f_u(k) \end{pmatrix}$$

$$r_k := \text{rank}(C_{\text{aug}}(k)). \quad (25)$$

At each sampling instant k, there is a matrix $P(k)$ that transforms matrix $C_{\text{aug}}(k)$ into the following form:

$$P(k)C_{\text{aug}}(k) = P(k)\begin{pmatrix} C_u^a(k) \\ \hat{C}_x^a(k+1)f_u(k) \end{pmatrix} = \begin{pmatrix} \tilde{C}_u^a(k) \\ 0 \end{pmatrix} \quad (26)$$

with $\tilde{C}_u^a(k) \in \mathbb{R}^{r_k \times m}$, which has independent rows. By defining

$$\Gamma(k) := \begin{pmatrix} P(k)\begin{pmatrix} C_x^a(k) \\ \hat{C}_x^a(k+1)f_u(k) \end{pmatrix} \\ \bar{C}_x^a(k) \end{pmatrix} \quad (27)$$

and assuming that γ_k is the number of rows of matrix $\Gamma(k)$, $\Gamma(k)$ can be partitioned into a block matrix as

$$\Gamma(k) = \begin{pmatrix} \tilde{C}_x^a(k) \\ \hat{C}_x^a(k) \end{pmatrix}.$$

We then obtain

$$\tilde{C}_x^a(k) = (I_{r_k \times r_k} \quad 0_{r_k \times (\gamma_k - r_k)})\Gamma(k) \in \mathbb{R}^{r_k \times m}$$
$$\hat{C}_x^a(k) = (0_{(\gamma_k - r_k) \times r_k} \quad I_{(\gamma_k - r_k) \times (\gamma_k - r_k)})\Gamma(k) \in \mathbb{R}^{(\gamma_k - r_k) \times m}.$$

By defining

$$\begin{aligned} Z_{11}(k) &:= H_{xx}(k) + f_x(k)^T S(k+1) f_x(k) \\ Z_{21}(k) &:= Z_{12}(k)^T = H_{ux}(k) + f_u(k)^T S(k+1) f_x(k) \\ Z_{22}(k) &:= H_{uu}(k) + f_u(k)^T S(k+1) f_u(k) \\ K_0(k) &:= \begin{pmatrix} Z_{22}(k) & \tilde{C}_u^a(k)^T \\ \tilde{C}_u^a(k) & 0 \end{pmatrix}^{-1} \qquad (28) \\ S(k) &:= Z_{11}(k) - \begin{pmatrix} Z_{12}(k) & \tilde{C}_x^a(k)^T \end{pmatrix} K_0(k) \begin{pmatrix} Z_{21}(k) \\ \tilde{C}_x^a(k) \end{pmatrix} \\ T(t+N) &:= 0 \\ T(k) &:= f_x(k)^T T(k+1) - \begin{pmatrix} Z_{12}(k) & \tilde{C}_x^a(k)^T \end{pmatrix} \\ &\quad \times K_0(k) \begin{pmatrix} f_u(k)^T T(k+1) + H_u(k) \\ 0 \end{pmatrix} \end{aligned}$$

where $Z_{22}(k) \succ 0$ for $k \in [t, t+N]$. Using $S(t+N)$ and $T(t+N)$ as the initial conditions for backward iteration, we calculate the matrix sequences described above. We then obtain the explicit relation between state and input variations of the perturbed solution as (12).

When δx_t is large and causes activity status changes in constraints, δx_t is divided into smaller segments and applied the NE solution to each segment. Details in handling changes in the activity status of constraints are addressed in [26], [27], and [35].

ACKNOWLEDGMENT

The authors would like to thank Gayathri Seenumani of GE Global Research for many interesting and inspiring discussions on the research reflected in this paper.

REFERENCES

[1] N. H. Doerry and J. C. Davis, "Integrated power system for marine applications," *Naval Eng. J.*, vol. 106, no. 3, pp. 77–90, 1994.

[2] N. Doerry and K. McCoy, "Next generation integrated power system: NGIPS technology development roadmap," Naval Sea Syst. Command, Washington, DC, USA, Tech. Rep. 0704-0188, 2007.

[3] G. Seenumani, "Real-time power management of hybrid power systems in all electric ship applications," Ph.D. dissertation, Dept. Mech. Eng., Univ. Michigan, Ann Arbor, MI, USA, 2010.

[4] S. Srivastava and K. L. Butler-Purry, "Expert-system method for automatic reconfiguration for restoration of shipboard power systems," *IEE Proc.-Generat., Transmiss., Distrib.*, vol. 153, no. 3, pp. 253–260, 2006.

[5] K. L. Butler-Purry and N. D. R. Sarma, "Self-healing reconfiguration for restoration of naval shipboard power systems," *IEEE Trans. Power Syst.*, vol. 19, no. 2, pp. 754–762, May 2004.

[6] J. M. Solanki and N. N. Schulz, "Using intelligent multi-agent systems for shipboard power systems reconfiguration," in *Proc. 13th Int. Conf. Intell. Syst. Appl. Power Syst.*, 2005, pp. 212–214.

[7] Y. Huang, "Fast reconfiguration algorithm development for shipboard power systems," M.S. thesis, Dept. Elect. Comput. Eng., Mississippi State Univ., Starkville, MS, USA, 2005.

[8] P. Mitra and G. K. Venayagamoorthy, "Real-time implementation of an intelligent algorithm for electric ship power system reconfiguration," in *Proc. IEEE Electr. Ship Technol. Symp.*, Apr. 2009, pp. 219–226.

[9] G. Seenumani, J. Sun, and H. Peng, "Real-time power management of integrated power systems in all electric ships leveraging multi time scale property," *IEEE Trans. Control Syst. Technol.*, vol. 20, no. 1, pp. 232–240, Jan. 2012.

[10] C. E. Garcia, D. M. Prett, and M. Morari, "Model predictive control: Theory and practice—A survey," *Automatica*, vol. 25, no. 3, pp. 335–348, 1989.

[11] S. J. Qin and T. A. Badgwell, "An overview of nonlinear model predictive control applications," in *Nonlinear Model Predictive Control*. Basel, Switzerland.: Birkhäuser Basel, 2000, pp. 369–392.

[12] S. J. Qin and T. A. Badgwell, "A survey of industrial model predictive control technology," *Control Eng. Pract.*, vol. 11, no. 7, pp. 733–764, 2003.

[13] R. Findeisen and F. Allgöwer, "Computational delay in nonlinear model predictive control," in *Proc. Int. Symp. Adv. Control Chem. Proces.*, 2004, pp. 427–432.

[14] L. Santos, P. Afonso, J. Castro, N. Oliveria, and L. Biegler, "On-line implementation of nonlinear MPC: An experimental case study," *Control Eng. Pract.*, vol. 9, no. 8, pp. 847–857, 2001.

[15] M. Diehl, H. J. Ferreau, and N. Haverbeke, "Efficient numerical methods for nonlinear MPC and moving horizon estimation," in *Nonlinear Model Predictive Control*. Berlin, Germany: Springer-Verlag, 2009, pp. 391–417.

[16] M. Cannon, "Efficient nonlinear model predictive control algorithms," *Annu. Rev. Control*, vol. 28, no. 2, pp. 229–237, 2004.

[17] B. Houska, H. J. Ferreau, and M. Diehl, "An auto-generated real-time iteration algorithm for nonlinear MPC in the microsecond range," *Automatica*, vol. 47, no. 10, pp. 2279–2285, 2011.

[18] M. Vukov, W. Van Loock, B. Houska, H. J. Ferreau, J. Swevers, and M. Diehl, "Experimental validation of nonlinear MPC on an overhead crane using automatic code generation," in *Proc. Amer. Control Conf.*, Jun. 2012, pp. 6264–6269.

[19] M. Diehl *et al.*, "Real-time optimization for large scale processes: Nonlinear model predictive control of a high purity distillation column," in *Online Optimization of Large Scale Systems*. Berlin, Germany: Springer-Verlag, 2001, pp. 363–383.

[20] M. Diehl, H. G. Bock, J. P. Schöder, R. Findeisen, Z. Nagy, and F. Allgöwer, "Real-time optimization and nonlinear model predictive control of processes governed by differential-algebraic equations," *J. Process Control*, vol. 12, no. 4, pp. 577–585, 2002.

[21] W. C. Li and L. T. Biegler, "Newton-type controllers for constrained nonlinear processes with uncertainty," *Ind. Eng. Chem. Res.*, vol. 29, no. 8, pp. 1647–1657, 1990.

[22] T. Ohtsuka, "A continuation/GMRES method for fast computation of nonlinear receding horizon control," *Automatica*, vol. 40, no. 4, pp. 563–574, 2004.

[23] V. M. Zavala and L. T. Biegler, "The advanced-step NMPC controller: Optimality, stability and robustness," *Automatica*, vol. 45, no. 1, pp. 86–93, 2009.

[24] M. J. Tenny, S. J. Wright, and J. B. Rawlings, "Nonlinear model predictive control via feasibility-perturbed sequential quadratic programming," *Comput. Optim. Appl.*, vol. 28, no. 1, pp. 87–121, 2004.

[25] R. Ghaemi, J. Sun, and I. Kolmanovsky, "Overcoming singularity and degeneracy in neighboring extremal solutions of discrete-time optimal control problem with mixed input-state constraints," in *Proc. 17th IFAC World Congr.*, 2009, pp. 1454–1459.

[26] R. Ghaemi, J. Sun, and I. V. Kolmanovsky, "An integrated perturbation analysis and sequential quadratic programming approach for model predictive control," *Automatica*, vol. 45, no. 10, pp. 2412–2418, 2009.

[27] R. Ghaemi, J. Sun, and I. V. Kolmanovsky, "A neighboring extremal approach to nonlinear model predictive control," in *Proc. 8th IFAC Symp. Nonlinear Control Syst.*, Sep. 2010, pp. 747–752.

[28] A. E. Bryson and Y.-C. Ho, *Applied Optimal Control: Optimization, Estimation and Control*. New York, NY, USA: Taylor & Francis, 1975.

[29] R. Ghaemi, "Robust model based control of constrained systems," Ph.D. dissertation, Dept. Elect. Eng., Univ. Michigan, Ann Arbor, MI, USA, 2010.

[30] C. Büskens and H. Maurer, "Sensitivity analysis and real-time control of parametric optimal control problems using nonlinear programming methods," in *Online Optimization of Large Scale Systems*. Berlin, Germany: Springer-Verlag, 2001, pp. 57–68.

[31] J. V. Kadam and W. Marquardt, "Sensitivity-based solution updates in closed-loop dynamic optimization," in *Proc. 7th Int. Symp. Dyn. Control Process Syst.*, vol. 7. 2004, pp. 947–952.
[32] V. M. Zavala, C. D. Laird, and L. T. Biegler, "Fast implementations and rigorous models: Can both be accommodated in NMPC?" *Int. J. Robust Nonlinear Control*, vol. 18, no. 8, pp. 800–815, 2008.
[33] C. J. Doktorcik, "Modeling and simulation of a hybrid ship power system," M.S. thesis, Dept. Elect. Comput. Eng., Purdue Univ., West Lafayette, IN, USA, 2010.
[34] M. Bash *et al.*, "A medium voltage DC testbed for ship power system research," in *Proc. IEEE Electr. Ship Technol. Symp.*, Apr. 2009, pp. 560–567.
[35] R. Ghaemi, J. Sun, and I. Kolmanovsky, "Model predictive control for constrained discrete time systems: An optimal perturbation analysis approach," in *Proc. Amer. Control Conf.*, 2007, pp. 3757–3762.
[36] J. Nocedal and S. J. Wright, *Numerical Optimization* (Operations Research and Financial Engineering). New York, NY, USA: Springer-Verlag, 2006.
[37] Y. Xie, R. Ghaemi, J. Sun, and J. S. Freudenberg, "Model predictive control for a full bridge DC/DC converter," *IEEE Trans. Control Syst. Technol.*, vol. 20, no. 1, pp. 164–172, Jan. 2012.
[38] H. Park, I. Kolmanovsky, and J. Sun, "Model predictive control of spacecraft relative motion maneuvering using the IPA-SQP approach," in *Proc. ASME Dyn. Syst. Control Conf.*, vol. 1. 2013, pp. V001T02A001.

Hyeongjun Park received the B.S. and M.S. degrees from Seoul National University, Seoul, Korea, in 2003 and 2008, respectively, and the Ph.D. degree from the University of Michigan, Ann Arbor, MI, USA, in 2014, all in aerospace engineering.

He was a Visiting Researcher with the Department of Aeronautics and Astronautics, University of Tokyo, Tokyo, Japan, in 2006. He was with the Department of Mechanical Engineering, Samsung Engineering Company, Ltd., Seoul, from 2008 to 2009. He is currently a Post-Doctoral Researcher with the Department of Aerospace Engineering, University of Michigan. His current research interests include real-time optimal control of constrained systems, control of spacecraft proximity operations, and power management control.

Jing Sun (F'04) received the B.S. and M.S. degrees from the University of Science and Technology of China, Hefei, China, in 1982 and 1984, respectively, and the Ph.D. degree from the University of Southern California, Los Angeles, CA, USA, in 1989.

She was an Assistant Professor with the Department of Electrical and Computer Engineering, Wayne State University, Detroit, MI, USA, from 1989 to 1993. She joined the Ford Research Laboratory, Department of Powertrain Control Systems, Dearborn, MI, USA, in 1993. After spending almost 10 years in the industry, she came back to academia and joined as a Faculty Member with the College of Engineering, University of Michigan, Ann Arbor, MI, USA, in 2003, where she is currently a Professor with the Department of Naval Architecture and Marine Engineering and the Department of Electrical Engineering and Computer Science. She has co-authored a textbook entitled *Robust Adaptive Control*, and holds over 30 U.S. patents. Her current research interests include system and control theory and its applications to marine and automotive propulsion systems.

Prof. Sun is one of the three recipients of the IEEE Control System Technology Award in 2003.

Steven Pekarek (F'13) received the B.S., M.S., and Ph.D. degrees in electrical engineering from Purdue University, West Lafayette, IN, USA, in 1991, 1993, and 1996, respectively.

He was an Assistant (Associate) Professor of Electrical and Computer Engineering with the University of Missouri, Rolla, MO, USA, from 1997 to 2004. He is currently a Professor of Electrical and Computer Engineering with Purdue University, and an Area Chair of Power and Energy Systems. He has been a Principal Investigator on a number of successful research programs, including projects for the Navy, Air Force, Ford Motor Company, Motorola, and Delphi Automotive Systems. The primary focus of these investigations has been the analysis and design of power electronic-based architectures for finite inertia power and propulsion systems.

Philip Stone (M'06) received the B.S., M.E., and Ph.D. degrees in electrical engineering from the University of South Carolina, Columbia, SC, USA, in 2005, 2008, and 2010, respectively. His graduate work was focused on power systems and power quality.

He has been with GE Power Conversion Naval Systems, Inc., Pittsburgh, PA, USA, where he has spent significant time on Navy related projects, such as the power management controller, which uses model predictive control to dynamically coordinate the sources and loads of a ship power system to minimize a cost function. He is currently a Lead Engineer/Technologist with GE Power Conversion Naval Systems, Inc., where he is focused on developing state-of-the-art high power and medium voltage solar inverters.

Daniel Opila (M'08) received the B.S. and M.S. degrees from the Massachusetts Institute of Technology, Cambridge, MA, USA, in 2002 and 2003, respectively, and the Ph.D. degree from the University of Michigan, Ann Arbor, MI, USA, in 2010.

He was a Senior Research and Development Engineer with GE Power Conversion Naval Systems, Inc., Pittsburgh, PA, USA. He was also a Visiting Scholar with Ford Motor Company, Dearborn, MI, USA, a Senior Engineer with Orbital Sciences Corporation, Dulles, VA, USA, and a Mechanical Engineer with Bose Corporation, Framingham, MA, USA. He is currently an Assistant Professor of Electrical and Computer Engineering with the United States Naval Academy, Annapolis, MD, USA. He is a licensed Professional Engineer in Pennsylvania and specializes in optimal control of energy systems, including hybrid vehicles, naval power systems, power converters, and renewables.

Richard Meyer received the B.S. and M.S. degrees from the University of Missouri, Rolla, MO, USA, in 1993 and 1995, respectively, and the Ph.D. degree from Purdue University, West Lafayette, IN, USA, in 2012, all in mechanical engineering.

He is currently with the School of Mechanical Engineering, Purdue University, West Lafayette, IN, USA. He was with Ford Motor Company, Dearborn, MI, USA, where he was involved in advanced transmission control system design. His current research interests include power management, hybrid systems, and model predictive control.

Mr. Meyer received the National Defense Science and Engineering Graduate Fellowship from Purdue University, and the National Science Foundation Fellowship.

Ilya Kolmanovsky (F'08) received the M.S. and Ph.D. degrees in aerospace engineering, and the M.A. degree in mathematics, all from the University of Michigan, Ann Arbor, MI, USA, in 1993, 1995, and 1995, respectively.

He has been with Ford Research and Advanced Engineering, Dearborn, MI, USA, for around 15 years. He is currently a Professor with the Department of Aerospace Engineering, University of Michigan. His current research interests include control theory for systems with state and control constraints, and control applications to aerospace and automotive systems.

Dr. Kolmanovsky was a recipient of the Donald P. Eckman Award of the American Automatic Control Council, and the IEEE TRANSACTIONS ON CONTROL SYSTEMS TECHNOLOGY Outstanding Paper Award.

Raymond DeCarlo (F'89) was born in Philadelphia, PA, USA. He received the B.S. and M.S. degrees in electrical engineering from the University of Notre Dame, Notre Dame, IN, USA, in 1972 and 1974, respectively, and the Ph.D. degree from Texas Tech University, Lubbock, TX, USA, in 1976, under the supervision of Dr. R. Saeks.

He joined Purdue University, West Lafayette, IN, USA, as an Assistant Professor of Electrical Engineering, in 1977, where he became an Associate Professor and a Full Professor in 1982 and 2005. He was with General Motors Research Laboratories, Detroit, MI, USA, in 1985 and 1986.

Dr. DeCarlo was an Associate Editor of Technical Notes and Correspondence, and Survey and Tutorial Papers of the IEEE TRANSACTIONS ON AUTOMATIC CONTROL. He was a Secretary Administrator of the IEEE Control Systems Society, a member of the Board of Governors from 1986 to 1992 and 1999 to 2003, the Program Chair of the IEEE Conference on Decision and Control (CDC) (Honolulu) in 1990, the General Chair of the IEEE CDC (San Antonio) in 1993, and the Vice President of the IEEE Control Systems Society of Financial Activities from 2001 to 2002.